

Chapter 12

Characterization of Hydrogen Trapping Systems and HIC Susceptibility of X60 Steel by Traditional and Innovative Methodologies



Renzo Valentini, Francesco Aiello, Linda Bacchi, Fabio Biagini, Serena Corsinovi, and Michele Villa

Abstract Hydrogen interaction with steels and metallic alloys, in general, is an old issue, but the interest in the phenomenon is incredibly increased in recent years. From the '90s of the last century up to today, the papers about Hydrogen Embrittlement (Scopus, Elsevier, Amsterdam, [1]) are almost tripled! This establishes the growing attention on this topic, due also to the development of hydrogen-based economy. In Oil & Gas industry, hydrogen–steel interaction and related phenomena are often related to corrosion reactions, a consequence of the severe sour environments typical of this industrial sector. This is the reason why corrosion is the second most frequent cause of pipeline failures (Yang et al., *Reliab Eng Syst Saf* 159, 214–222, [2]), with the peculiar result of dangerous substances released in the environment, and it has translated into a continuous development of new technologies to monitor and control the ‘corrosion state’. The present work aims at characterizing the hydrogen susceptibility of X60 steel, a High-Strength Low-Alloy (HSLA) steel, widely used in Oil & Gas industry. The study is carried out by means of a rigorous approach based on traditional scientific techniques; moreover, an innovative solution was developed, validated and proposed to approach the possibility of on-field monitoring of operating pipelines.

Keywords Hydrogen embrittlement · Hydrogen-induced cracking · X60 · Pipeline steels · Sour environment · Hydrogen trapping · Hydrogen diffusion

R. Valentini (✉) · F. Aiello
Department of Civil and Industrial Engineering, University of Pisa, 56122 Pisa, Italy
e-mail: renzo.valentini@unipi.it

L. Bacchi · F. Biagini · S. Corsinovi · M. Villa
Letomec SRL, 56126 Pisa, Italy

© The Author(s), under exclusive license to Springer Nature Switzerland AG 2021
V. A. Polyanskiy and A. K. Belyaev (eds.), *Advances in Hydrogen Embrittlement Study*,
Advanced Structured Materials 143, https://doi.org/10.1007/978-3-030-66948-5_12

12.1 Introduction

Hydrogen embrittlement is a phenomenon of great interest for Oil&Gas industry, due to the use of higher grades steels, as well as low-purity service fluids, containing H_2S , for example. In this scenario, the possibility of approaching the plants and pipelines on-field monitoring looks very attractive and could be the real turning point for reducing failures and manage safe planned maintenance.

The mechanisms of hydrogen embrittlement and hydrogen interaction with metal lattice are still under investigation, but some theories are overall accepted to demonstrate the dangerous and deteriorating outcome of hydrogen absorption on steels' mechanical properties and behaviour. Nevertheless, the effect of hydrogen is mainly and deeply investigated for low-carbon steels, stainless steels, TRIP steels, DP steels, pipeline steels and so on [3], it is well known that the embrittlement effect is particularly severe for high-strength and ultra-high-strength steels. Typically, a UTS higher than 1000 MPa is assumed as threshold value to significantly appreciate it.

The most diffused models that describe the hydrogen embrittlement in metals are the HELP (Hydrogen-Enhanced Local Plasticity) and HEDE (Hydrogen-Enhanced DEcohesion). These models are quite different, HELP is related to hydrogen enhancement of dislocations' generation and motion, giving rise to local plasticized zones and material softening. Other literature studies state the opposite phenomenon, that is the pinning of dislocations due to the presence of hydrogen atoms. Katzarov et al. [4] and Taketomi et al. [5] observed and demonstrated the coexistence of both actions. Hydrogen affects dislocation mobility as a function of several factors, including hydrogen concentration, tension stress state and temperature. HEDE model is instead based on the reduction of metal lattice chemical bounds due to the presence of hydrogen, which promotes crack formation and propagation. It is strictly correlated to locally reach the critical hydrogen concentration.

Currently, the most recent researches propose a new approach which consists of the synergistic contribution of HELP and HEDE theories, the so-called HELP-mediated HEDE model [6]. A first HELP stage is followed by a combination of HELP and HEDE mechanisms, where hydrogen enhances the mobility of dislocations (HELP), giving rise to high-density dislocations pile up and plasticization at the crack tip. At the same time, hydrogen transportation by dislocation increases the local concentration in the metal leading to decohesion of chemical bonds (HEDE).

Hydrogen-induced cracking (HIC) is another phenomenon typical of Oil & Gas industry. It usually takes place near to precipitates or non-metallic inclusions, vacancies or other microstructural defects, and consists in crack nucleation and propagation even without applied load to the part or component. When hydrogen accumulates in these areas, it can recombine into molecular hydrogen and reach a local overpressure level able to crack the metal according to hydrogen pressure theory [7].

Peng et al. [7] stated the HIC nucleation depends on the type and shape of the inclusions: MnS, as well as Al, Ti and Ca oxides, are very active initiation sites, while inclusions rich in Si present a low risk. Recent studies [7] showed a better resistance

of pipeline steels with controlled precipitation of carbides and nitrides (as V_4C_3 , TiC, NbC and nanosized (Ti,Mo,C) aimed at reducing particles size and increasing their number [8].

Sour environment, typical of petrochemical plants, is characterized by the presence of a strongly reactive and dangerous compound, the hydrogen sulphide. H_2S inhibits the recombination of atomic hydrogen into molecular hydrogen according to the following reactions:



Equation (12.3) allows atomic hydrogen to be adsorbed on the metal surface, considerably increasing the probability of absorption in the bulk material and the risk of hydrogen damage [9].

12.2 Materials and Methods

The present work focuses on API X60 and Iron-Armco $\text{\textcircled{S}}$. API X60 is HSLA pipeline steel that combines good resistance, ductility, weldability and corrosion resistance. The strengthening mechanisms consist of the partial precipitation of inclusions, coupled with grain size reduction and it is subjected to hot rolling. Fe Armco is instead cold rolled and annealed. Mechanical properties and chemical compositions are listed in Tables 12.1 and 12.2 respectively.

For permeation tests, rectangular sheet specimens of different thickness (0.5, 1 and 2 mm) were used, for HIC tests and TPD analyses, cylindrical specimens were manufactured, of diameter, respectively, 13 and 6 mm.

12.3 Experimental

A series of experimental tests were carried out in order to characterize the steel behaviour in a hydrogen environment and its susceptibility to hydrogen embrittlement.

Table 12.1 Mechanical properties of API X60

$R_{p0.2}$ (Mpa)	R_m (Mpa)	Elongation (%)
436	520	40

Table 12.2 Composition of Iron Armco § and API X60

	API X60	Fe Armco
C	0.1343%	0.01%
Mn	1.15%	0.15%
Si	0.2523%	–
S	0.0047%	0.015%
P	0.0217%	0.015%
Al	0.0254%	0.05%
Ti	0.022%	–
Nb	0.038%	–
N	0.0102%	0.007%
Fe	Balance	Balance

12.3.1 Permeation Tests

Permeation tests were performed to evaluate hydrogen diffusion in steels, determining the hydrogen diffusion coefficient.

The traditional test method, based on Devanathan–Stachurski double cell [10], was used. The Devanathan–Stachurski technique involves the application of a Pd coating to the sample surface. A solution of PdCl₂ (5 g/L) and NH₃ (28% in volume) was used and a current density of 4 mA/cm² [11] was applied, after a prior surface polish. The sample is placed between two semi-cells and surface passivation of one side is achieved by using 0.1 N NaOH solution and imposing 200 mV with respect to Ag/AgCl reference electrode.

Permeation tests were also carried out by means of HELIOS 2 (Hydrogen Embrittlement Line Instruments and Operative Sensors), an innovative equipment patented by Letomec S.r.l [12] (patent EP2912452B1), and results were compared.

HELIOS 2 is based on an electrochemical cell, where the metallic sample, the cathode, is in contact with the electrolytic solution through a hole in the cell with calibrated diameter. Applying a certain current between the anode and the cathode, hydrogen is produced on the exposed surface of the sample. A probe, containing a solid-state gas sensor, registers the hydrogen flux coming out from the other side (see Fig. 12.1). HELIOS method since there is no electrolytic solution on the detection side, doesn't require the passivation of the metallic sample.

After the preliminary comparison among Devanathan and HELIOS 2 methods on the reference material (Iron Armco), permeation tests were repeated on API X60 HSLA steel. Tests were executed by varying operative temperature, to estimate the low-energy traps binding energy and, in a second phase, tests on samples with different thicknesses were executed. Finally, for what concerns permeation tests, a real case of cracking was simulated. A sheet of 2 mm thickness has been put in contact with H₂SO₄ 1 N and As₂O₃ 10 mg/L and a current density of 50 mA/cm² was applied.

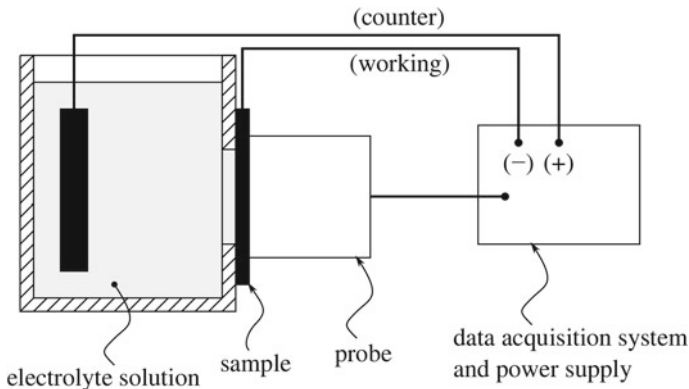


Fig. 12.1 Helios 2 equipment scheme

12.3.2 TPD Tests

Hydrogen trapping systems were studied by the temperature-programmed desorption technique. Pre-charged samples were heated from room temperature up to 600 °C. Various heating rates were applied, and binding energy of traps was extrapolated. According to Choo and Lee model [13], the heating rate can be expressed as follows:

$$\dot{z} = A(1 - z)e^{E_a/RT} \tag{12.4}$$

with $z = (C_0 - C(t))/C_0$ and where C_0 and $C(t)$ represent, respectively, the initial and the instantaneous hydrogen concentration in steel, A is a proportionality constant, R the gas constant, T the absolute temperature and E_a the activation energy of a trap. Deriving the Equation (12.4), the following expression is obtained:

$$\frac{d\dot{z}}{dt} = -A\dot{z}e^{-\frac{E_a}{RT}} + A(1 - z)e^{-\frac{E_a}{RT}} \frac{E_a}{RT^2} \frac{dT}{dt} \tag{12.5}$$

imposing $\frac{d\dot{z}}{dt} = 0$, the maximum of the function ($\frac{dT}{dt} = \phi$) can be determined.

$$-A\dot{z}e^{-\frac{E_a}{RT_p}} + \dot{z} \frac{E_a}{RT_p^2} \phi = 0 \quad (T_p = \text{Peak Temperature}) \implies -\frac{E_a}{RT_p} = \ln \left[\left(\frac{E_a}{ART_p^2} \right) \phi \right] \tag{12.6}$$

In a diagram where $\left(\frac{1}{T_p}; \ln \left[\left(\frac{\phi}{T_p^2} \right) \right] \right)$ were plotted, experimental points settle on a straight line and the binding energy can be estimated from the slope of that line.

12.3.3 HIC Tests

HIC is an extremely dangerous and unpredictable phenomenon, related to corrosion phenomena and consequent hydrogen absorption in the metal lattice. There are a lot of factors influencing HIC phenomenon like environment, microstructure, shape of the grain boundaries, number and type of inclusions [14].

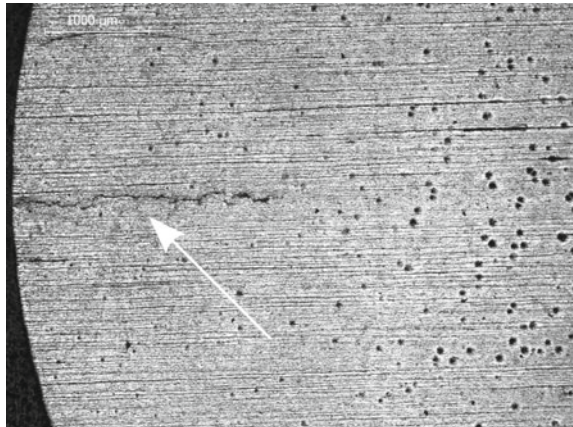
That is why, a series of HIC nucleation tests were carried out, in order to determine the critical hydrogen concentration able to give rise to crack initiation. Samples were electrochemically charged by varying electrolytic solution and current density to introduce a different amount of hydrogen in the metal lattice, then they were cut into two parts. A half was observed under light microscope to check the presence of cracks, the other half was used for hydrogen measurement by means of thermal desorption analysis. Figure 12.2 shows an example of cracked material in a hydrogen-induced cracking test.

12.3.4 Numerical Analysis

A series of numerical simulations were also performed to determine hydrogen trapping parameters in the bulk steel. Typical diffusion behaviour, explained by Fick's law [15, 16], is not verified in the presence of hydrogen trapping sites in the metal lattice. McNabb and Forster developed a theory to consider this effect and this was implemented in a simulation model to determine all kinetic parameters [17].

$$\begin{cases} \frac{\partial C}{\partial t} = D \frac{\partial^2 C}{\partial x^2} - N_r \frac{\partial v}{\partial t} - N_i \frac{\partial w}{\partial t} \\ \frac{\partial v}{\partial t} = k_r C(1 - v) - p v \\ \frac{\partial w}{\partial t} = k_i C t(1 - w) \end{cases} \quad (12.7)$$

Fig. 12.2 API X60 sample, hydrogen crack was highlighted with the white arrow



where C and D are the hydrogen concentration and the diffusion coefficient, respectively; N_r and N_i are the reversible and irreversible traps concentration, ν is the occupied reversible trap fraction, w the irreversible one; k_r is the reversible trapping rate, k_i the irreversible one and p is the release amount for reversible traps.

Solve Eq. 12.7, combined with the corresponding initial and boundary conditions, allows to determine the outlet hydrogen flux defined as $J(t) = -D\partial_x C$. The initial conditions correspond to reversible and irreversible traps initially empty and material free of diffusible hydrogen. Boundary conditions consist of a constant concentration C_0 on the face of the specimen in contact with the electrolyte solution and zero concentration on the opposite face. The mathematical formulation is reported in Eq. (12.8) and Eq. (12.9), respectively, where a is the sample thickness.

$$C(t = 0, x) = 0; \quad \nu(t = 0, x) = 0; \quad w(t = 0, x) = 0 \quad (12.8)$$

$$C(t, x = 0) = C_0; \quad C(t, x = a) = 0 \quad (12.9)$$

The hydrogen outlet flux is a function of time and seven other parameters C_0 , D , k_r , N_r , N_i , k_i , p . The iron lattice diffusion coefficient is constant at room temperature and equivalent to $7 \cdot 10^{-9}$ m²/s [18]. C_0 can be easily obtained from the hydrogen flow during steady state. The k_r/p ratio can be determined from the knowledge of the lattice number of sites per unit of volume N_L and from the activation energy of traps E_a known by the TPD technique using Eq. (12.10) [19].

$$\frac{k_r}{p} = \frac{1}{N_L} \exp\left(\frac{E_a}{RT}\right) \quad (12.10)$$

The remaining parameters were determined by minimizing the cost function f defined in Eq. 12.8.

$$F = \min[J_{\text{simulated}} - J_{\text{experimental}}]^2 \quad (12.11)$$

12.4 Results

12.4.1 Permeation Tests

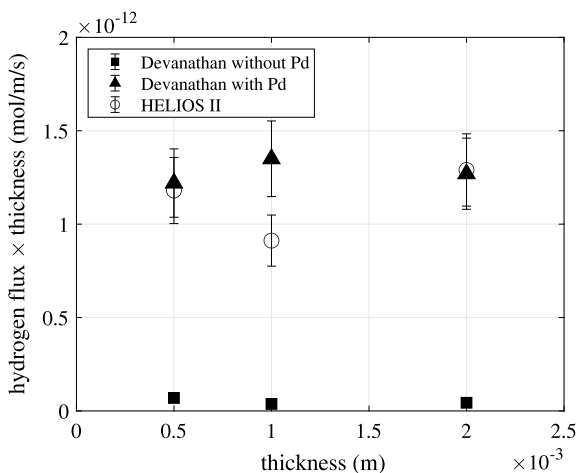
Permeation experiments were first executed on Iron Armco. Samples were tested with Devanathan method, with and without Pd coating, besides HELIOS 2 technique on bare specimens. Results were presented in Table 12.3.

Note that Palladium coating on the reading side is widely shown and demonstrated in the international literature to be a fundamental feature to get significant results [11], and this effect is clearly confirmed in Fig. 12.3.

Table 12.3 Permeations test results obtained with different detecting techniques on Fe-Armco

Thickness (m)	Material	J (mol/ms)	D (m ² /s)
0.0005	Fe D	$6.96 \cdot 10^{-14}$	$1.42 \cdot 10^{-10}$
	Fe + Pd D	$1.22 \cdot 10^{-12}$	$1.23 \cdot 10^{-10}$
	Fe H	$1.18 \cdot 10^{-12}$	$7.76 \cdot 10^{-11}$
0.001	Fe D	$3.74 \cdot 10^{-14}$	$2.45 \cdot 10^{-10}$
	Fe + Pd D	$1.35 \cdot 10^{-12}$	$4.60 \cdot 10^{-10}$
	Fe H	$9.12 \cdot 10^{-13}$	$2.22 \cdot 10^{-6}$
0.002	Fe D	$4.38 \cdot 10^{-14}$	$1.35 \cdot 10^{-9}$
	Fe + Pd D	$1.27 \cdot 10^{-12}$	$1.38 \cdot 10^{-9}$
	Fe H	$1.29 \cdot 10^{-12}$	$8.87 \cdot 10^{-10}$

Fig. 12.3 Comparison of exiting hydrogen flux in three different test conditions and for various sample thicknesses



12.4.1.1 API X60 Steel

Helios test results as a function of temperature were shown in Fig. 12.4. From these tests, the binding energy of the traps [20] was extrapolated and resulted equal to 18 kJ/mol.

Figure 12.5 indicated the stationary hydrogen flux determined during experimental results as a function of sample thickness.

Another test performed has been the permeation in crack condition (cracking conditions evaluated from HIC studies): so the conditions in terms of solution and current density able to generate microvoids due to the hydrogen interaction with metal lattice.

The permeation curve through the metal wall of the cracking case was reported in Fig. 12.6.

Fig. 12.4 Permeation tests at different temperatures

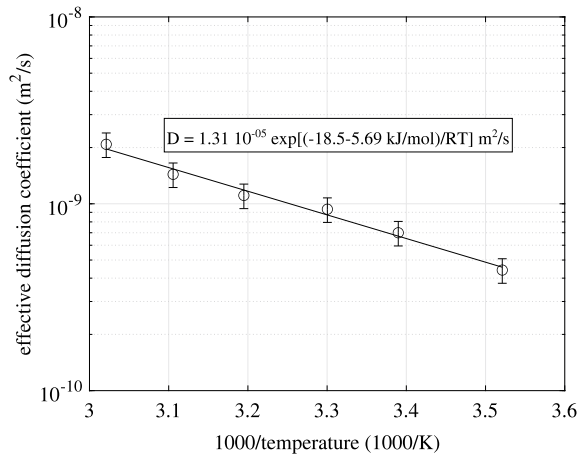
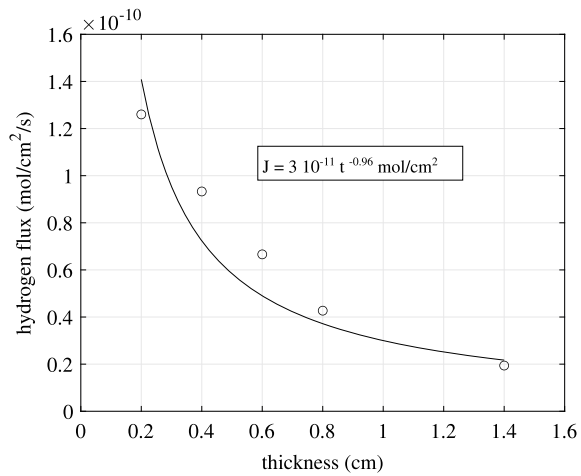


Fig. 12.5 Hydrogen flux varying sample's thickness



After reaching the maximum (point 1 in Fig. 12.6), the hydrogen signal decreases as an effect of crack nucleation: hydrogen accumulates in the cracks, while the amount exiting from the sheet decreases (point 2); when the new traps are filled the permeation flux starts to increase again and the signal goes up (point 3). Once determined the hydrogen concentration in steel, correspondent to the maximum peak of Fig. 12.6 (5.1 ppmw), and with reference to Fig. 12.7, the hydrogen accumulation next to the crack can be calculated. Considering the theoretical profile of hydrogen concentration along with the specimen thickness during permeation, [21] (Fig. 12.7(a)), the relationship between thickness and hydrogen concentration can be assumed linear:

$$C_H = C_{H,0} \left(1 - \frac{x}{L}\right) \tag{12.12}$$

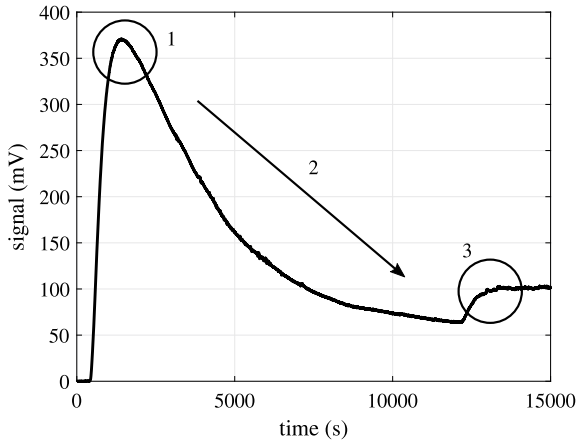


Fig. 12.6 Permeation in crack condition

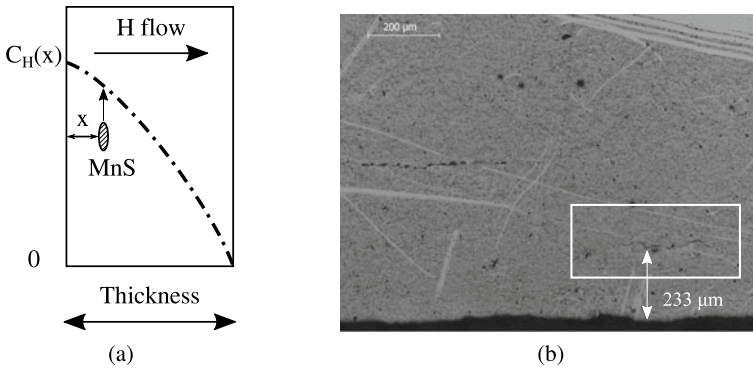


Fig. 12.7 **a** Hydrogen concentration profile and **b** crack and its distance from sample surface

where $C_{H,0}$ is the hydrogen concentration on the input surface, 5.1 ppmw (found from the HIC tests, where the sample was saturated, so the surface concentration is equal to the core one); x is the distance shown in Fig. 12.7(b) and L the sample thickness (2 mm). Given these considerations, C_H was estimated equal to 4.6 ppmw, and the result was in accordance with HIC results, shown in the following paragraphs.

Figure 12.8 shows the permeation curve of 2 mm thickness sample returned by HELIOS 2. The outgoing hydrogen flux, measured by the device, is represented as a function of time. Signal steady state is equal to $9.4 \cdot 10^{-6}$ mol/s m² and the curve was also used to identify the diffusion parameters through the previously exposed numerical model.

Fig. 12.8 Permeation curve obtained using HELIOS 2 on a 2mm thick sample

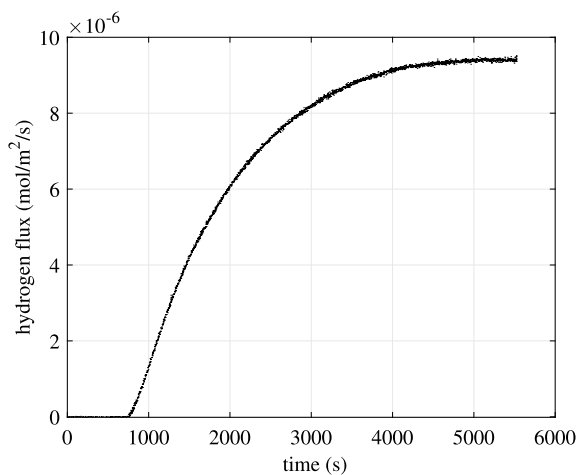
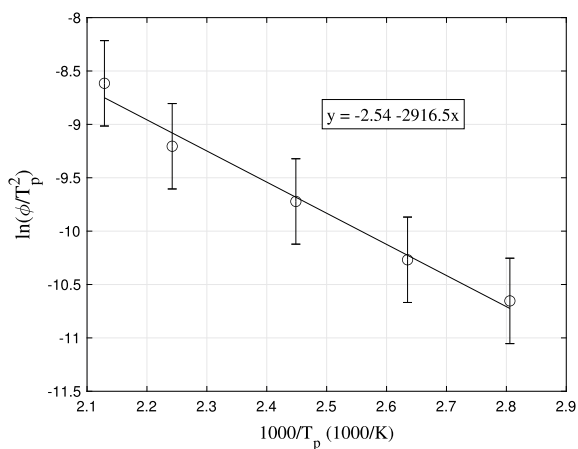


Fig. 12.9 TPD test results

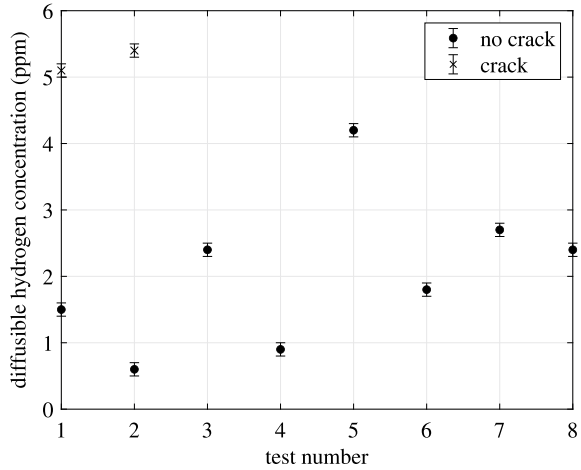


12.4.2 TPD Tests

Different heating rates have been set for TPD analysis: 2, 5, 10 and 20 °C/min. The results were plotted in Fig. 12.9, according to the model of Choo et Lee [13].

According to paragraph 12.3.1, starting from the slope of regression line, the binding energy can be easily estimated and it was equal to 24 kJ/mol.

Fig. 12.10 Results of HIC tests on API X60 steel



12.4.3 HIC Tests

HIC tests were carried out on cylindrical samples, after electrochemical hydrogen charging. Coupons were both observed by metallographic analysis to check the presence of cracks and in parallel the hydrogen content was determined by TDA.

The critical hydrogen concentration was estimated to be equal to 4.5 ppmw: this is the hydrogen amount able to crack the material without external load or applied stresses (Fig. 12.10).

12.4.4 Numerical Analysis

Starting from experimental data on API X60 steel with thickness 2 mm, a series of studies were carried out by numerical analysis. Figure 12.11 shows the comparison between the permeation experimental curve and the simulated one. The model allowed to calculate the occupancy of reversible traps. Figure 12.12 shows instead the simulated percentage occupancy of reversible traps as a function of the spatial coordinate for different permeation times. As can be seen, the occupancy of reversible traps remains small over time. The fractional occupation of the trap much smaller than one during the permeation test. Table 12.4 shows the diffusion and trapping parameters obtained by the simulation.

Equation (12.13) is a kinematic expression of Oriani's effective diffusion coefficient derived from the local equilibrium between atomic populations in the normal lattice and traps when the occupancy of trapping sites is very low [22].

$$D_{\text{eff}} = D \left(1 + N_r \frac{k_r}{p} \right)^{-1} \quad (12.13)$$

Fig. 12.11 Permeation curve. Comparison with the simulated one

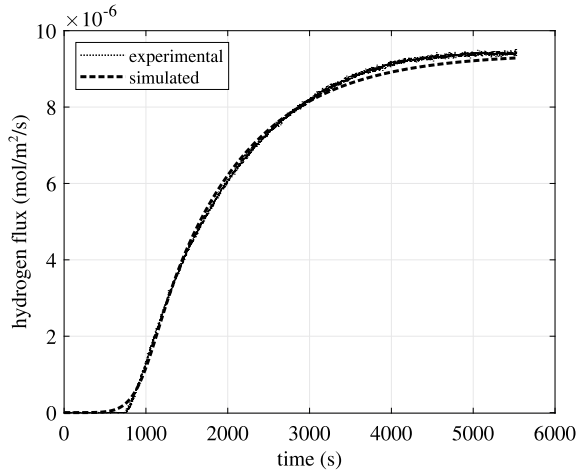


Fig. 12.12 Simulated percentage occupancy of reversible traps at different test times

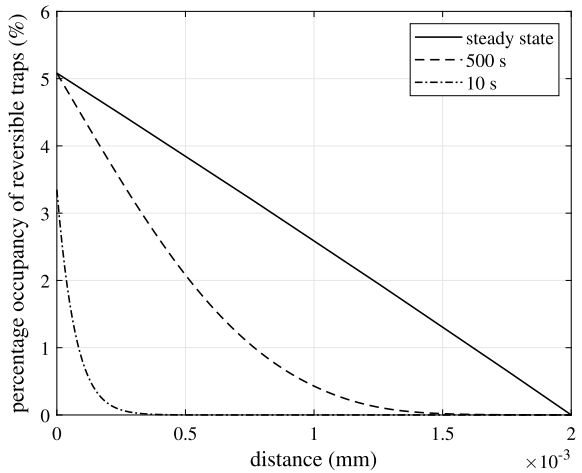


Table 12.4 Diffusion and trapping parameters identified by the permeation test

C_0 (mol/m ³)	N_r (mol/m ³)	N_i (mol/m ³)	k_r (m ³ /(mol s))	k_i (m ³ /(mol s))	p (1/s)
2.6	$9.1 \cdot 10^2$	1.3	$2.4 \cdot 10^{-3}$	$2.0 \cdot 10^{-1}$	$1.1 \cdot 10^{-1}$

The reversible trap concentration calculated using the Oriani model leads to a value equal to 210 mol/m³. This value is of the same order of magnitude as that identified by the numerical model.

12.5 Discussion

Pd coating is typically applied for Devanathan–Stachurcki permeation tests, it avoids the recombination of hydrogen atoms into molecular hydrogen before their oxidation in H^+ (electron release), with consequent reduction of detected current in the reading semi-cell.

In this case, the hydrogen flux exiting from the sample surface can be calculated as follows:

$$J_{De} = \frac{i}{F} \quad (12.14)$$

where i is the current density and F the Faraday's constant. Considering the results of Table 12.3, it can be noticed that without the Pd coating the underestimation of hydrogen flux and concentration is not negligible.

HELIOS 2 working principle is different and there is no need for Pd surface deposition since hydrogen escaping out of the metallic sample after recombination into molecular H_2 reacts with a solid-state gas sensor. This case shows the variation of sensor resistivity which returns an electrical signal in volts. Translating the signal into a hydrogen concentration and flux, the comparison with Devanathan method was possible and is reported in Fig. 12.3i

The flux through HELIOS 2 probe was calculated after a calibration of the instrument, evaluating molar amount per second in stationary conditions:

$$J_{He} = \frac{n}{A} \quad (12.15)$$

with A is the sample area in contact with the probe. HIC tests highlighted a good resistance to hydrogen damage of API X60 steel. Even though the quality of steel manufacturing can play a crucial role, a critical value near 4.5 ppmw was found. The result was also validated by the permeation test in severe environment, where the hydrogen flux was registered, and crack nucleation was identified through the sensor signal progress.

12.6 Conclusion

Devanathan-Stachurski method can be used for the calculation of hydrogen diffusion coefficient, but the Palladium coating deposition is needed for a reliable estimation of hydrogen flux coming out of the sample, especially for high values of hydrogen flux. This pointed out the elevated precision of the double cell for laboratory investigation but also the impossibility to apply the method to a real pipeline.

HELIOS technique, based on a solid-state gas sensor, is demonstrated to be very practical. Thanks to the high sensitivity device it can be applied directly to the pipe

wall. The laboratory investigation carried out in the present study, was aimed at approaching and validating the first step toward online monitoring.

The measurement carried out with HELIOS II of the hydrogen outlet flux was interpreted through a hydrogen diffusion and trapping numerical model providing results in line with the classical theory.

However, the realization of permeation tests with Devanathan-Stachurski on Pd coated specimens, can be successfully used for calibration and validation alternative methods.

Through the TPD and HIC tests, it has been possible a complete characterization of the material in terms of hydrogen trapping and binding energy [23] and the critical hydrogen concentration giving rise to cracks in the material.

Furthermore, the validation of new sensors and hydrogen evaluation suitable for the industrial application have been carried out and achieved.

References

1. Scopus. Elsevier, Amsterdam. <http://www.scopus.com> (2004). Accessed 16 June 2020
2. Yang, Y., Khan, F., Thodi, P., Abbassi, R.: Corrosion induced failure analysis of subsea pipelines. *Reliab. Eng. Syst. Safety*. **159**, 214–222 (2016)
3. Djukic, M., Bakic, G., Zeravic, V., Sedmak, A., Rajicic, B.: The synergistic action and interplay of hydrogen embrittlement mechanisms in steels and iron: localized plasticity and decohesion. *Eng. Fract. Mech.* **216**, 106528 (2019)
4. Katzarov, I., Pashov, D. L., and Paxton, A.: Hydrogen embrittlement I. Analysis of hydrogen-enhanced localized plasticity: effect of hydrogen on the velocity of screw dislocations in α -Fe. *Phys. Rev. Mater.* **1**, 1–11 (2017)
5. Taketomi, S., Matsumoto, R., Hagihara, S.: Molecular statics simulation of the effect of hydrogen concentration on 112 <111>edge dislocation mobility in Alpha Iron. *ISIJ Int.* **57**, 2058–2064 (2017)
6. Gerberich, W., Stauffer, D. and Sofronis, P.: A coexistent view of hydrogen effects on mechanical behaviour of crystals: HELP and HEDE effects of hydrogen on materials. In: Somerday, B., Sofronis, P., Jones, P. (eds.) *Effects of hydrogen on materials: proceedings of 2008 international hydrogen conference Jackons Lake Lodge, Grand Teton National Park, Wyoming, USA* (2008)
7. Peng, Z., Liu, J., Huang, F., Hu, Q., Cao, C., Hou, S.: Comparative study of non-metallic inclusions on the critical size for HIC initiation and its influence on hydrogen trapping. *Int. J. Hydrogen Energy* **45**, 12616–12628 (2020)
8. Pressouyre, G., Bernstein, I.: An example of the effect of hydrogen trapping on hydrogen embrittlement. *Metall. Trans. A* **12A**, 835–844 (1981)
9. Fragiél, A., Serna, S., Malo-Tamayo, J., Silva, P., Campillo, B., Martínez-Martínez, E., Cota, L., Staia, M., Puchi-Cabrera, E. and Perez, R.: Effect of microstructure and temperature on the stress corrosion cracking of two microalloyed pipeline steels in H₂S environment for gas transport. *Eng. Fail. Anal.* **105**, 1055–1068 (2019)
10. ISO 17081:2014: Method of measurement of hydrogen permeation and determination of hydrogen uptake and transport in metals by an electrochemical technique. ISO, Geneva (2004)
11. Manolatos, P., Jerome, M.: A thin palladium coating on iron for hydrogen permeation studies. *Electrochim. Acta* **41**, 359–365 (1996)
12. Valentini, R.: Methods for permeation hydrogen measurement. Patent EP2912452, 7 Dec 2012
13. Choo, W., Lee, J.: Thermal analysis of trapped hydrogen in pure iron. *Metall. Trans. A* **13A**, 135–140 (1982)

14. Pourazizi, R., Mohtadi-Bonab, M., Szpunar, J.: Role of texture and inclusions on the failure of an API X70 pipeline steel at different service environments. *Mater. Charact.* **164**, 110330 (2020)
15. Manolatos, P., Jerome, M., Duret-Thual, C., Le Coze, J.: The electrochemical permeation of hydrogen in steels without palladium coating. Part I: interpretation difficulties. *Corros. Sci.* **37**, 1773–1783 (1995)
16. Mehrer, H.: *Diffusion in solids*. Springer, Berlin (2007)
17. McNabb, A., Foster, P.K.: A New Analysis of the diffusion of hydrogen in iron and ferritic steels. *Trans. Metall. Soc.* **227**, 618–627 (1963)
18. Hagi, H., Hayashi, Y., Ohtani, N.: Diffusion coefficient of hydrogen in pure iron between 230 and 300K. *Trans. Jpn. Inst. Met.* **20**, 349–357 (1979)
19. Nagumo, M.: *Fundamentals of hydrogen embrittlement*. Springer, Singapore (2016)
20. Skjellerudsveen, M., Akselsen, O., Olden, V., Johnsen, R., Smirnova, A.: Effect of microstructure and temperature on hydrogen diffusion and trapping in X70 grade pipeline steel and its weldments. In: Presented at the second European Corrosion Congress, vol. 13–17. Moscow (September 2010)
21. Crank, J.: *The mathematics of diffusion*. Oxford University Press, London and New York (1957)
22. Oriani, R.: The diffusion and trapping of hydrogen in steel. *Acta Metal.* **18**, 147–157 (1970)
23. Villa, M.: *Controllo dei fenomeni di HE nei tubi in acciaio per oil and gas: applicazione di sistemi innovativi di monitoraggio*. Dissertation, University of Pisa (2018)